Supporting information to

Sulfur depletion through repetitive redox cycling unmasks the role of the cryptic sulfur cycle for (methyl)thioarsenate formation in paddy soils

José M. León Ninin[1*], Carolin Dreher[2], Andreas Kappler[2], Britta Planer-Friedrich[1‡]

[1] Environmental Geochemistry, Bayreuth Center for Ecology and Environmental Research (BayCEER), University of Bayreuth, 95440 Bayreuth, Germany

[2] Geomicrobiology, Department of Geosciences, University of Tübingen, 72076 Tübingen, Germany

* Corresponding author. Phone: +49-921-553995; E-mail address: jose.leon-ninin@uni-bayreuth.de (J.M. León Ninin).

‡ Deceased

(8 Pages, 3 Tables, 12 Figures)

Supplementary Data

Table S1: Selected soil properties of the original soil used for the long-term incubation experiment.

Soil name	Horizon*	Horizon depth (cm)*	Soil pH*	Soil Org. C* (g kg^{-1})	Soil Fe* (g kg^{-1})	Soil As** (mg kg^{-1})	Soil S** (g kg^{-1})	Fe_O/Fe_{DCB}**
P50	Alp1	0 - 7	7.4	17.8 ± 0.5	38	17	3.52	0.43 ± 0.04

*Data from Kölbl, Schad (1). **Data from León Ninin, Muehe (2). Oxalate extractable iron (Fe_O), Dithionate-citrate-bicarbonate extractable iron (Fe_{DCB}).

Table S2: Parameters collected during Mössbauer spectra analysis.

Sample	Phase	CS (mm/s)	QS/ ε (mm/s)	H (T)	σ*	Relative area (%)	χ^2
C0 (77 K)	$Fe^{III}_{adsorbed}$/clays	0.46	0.72			**52.6**	0.64
	Fe^{II}_{total}	1.24	2.87			30.1	
	Crystalline Fe^{III}(oxyhydr)oxides	0.39	-0.17	52.1	3.0	17.3	
C0 (5 K)	Fe(III)/clays	0.48	0.72			**45.5**	0.77
	Fe^{II}	1.30	2.81			27.2	
	Crystalline Fe^{III}(oxyhydr)oxides	0.49	-0.08	51.9	3.0	24.5	
	Poorly crystalline Fe^{III}(oxyhydr)oxides	0.35	-0.14	48.0	0.0	2.8	
C10 (77 K)	Fe^{III}/clays	0.47	0.73			**52.1**	0.52
	Fe^{II}	1.23	2.84			33.6	
	Crystalline Fe^{III}(oxyhydr)oxides	0.53	-0.071	51.9	2.2	14.3	
C10 (5 K)	Fe^{III}/clays	0.42	0.73			**53.8**	0.79
	Fe^{II}	1.30	2.79			28.0	
	Crystalline Fe^{III}(oxyhydr)oxides	0.53	-0.072	51.9	2.2	12.8	
	Poorly crystalline Fe^{III}(oxyhydr)oxides	0.35	0.019	58.4	3.0	5.4	
C30 (77 K)	Fe^{III}/clays	0.44	0.71			**50.7**	0.55
	Fe^{II}	1.24	2.84			32.1	
	Crystalline Fe^{III}(oxyhydr)oxides	0.43	-0.069	51.5	2.3	17.2	
C30 (77 K)	Fe^{III}/clays	0.48	0.71			**53.3**	0.83
	Fe^{II}	1.30	2.78			30.4	
	Crystalline Fe^{III}(oxyhydr)oxides	0.43	-0.14	51.5	2.3	9.5	
	Poorly crystalline Fe^{III}(oxyhydr)oxides	0.33	-0.034	49.1	3.0	6.8	

Center shift (CS), quadrupole splitting (QS), hyperfine field (H), sigma, the relative area and the goodness of the fit χ^2.

Table S3: Relative areas (%) of mineral phases and total Fe content in samples C0, C10, and C30.

Mineral phase & Fe soil content	C0	C10	C30
$Fe^{III}_{adsorbed}$/clays	45.5	53.8	53.3
Fe^{II}_{total}	27.2	28.0	30.4
Crystalline Fe^{III}(oxyhydr)oxides	24.6	12.8	9.5
Poorly Crystalline Fe^{III}(oxyhydr)oxides	2.8	5.4	6.8
Total Fe content (g kg^{-1})	33 ± 2	27 ± 2	23 ± 1

Values for Total Fe content in the soil are given as average ± standard deviation (n = 3).

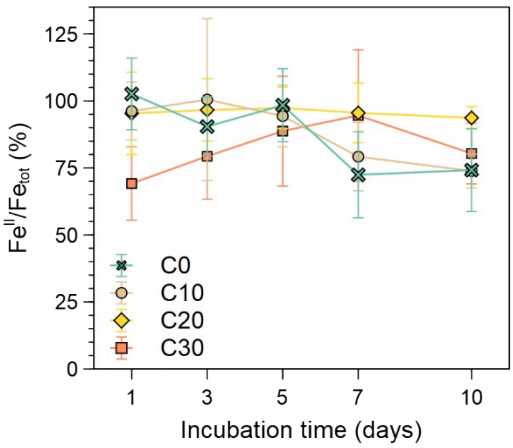

Figure S1: Fraction of reduced Fe in total dissolved Fe throughout incubation time for all redox cycled soils. Data points are average values and bars indicate standard deviation (n = 3).

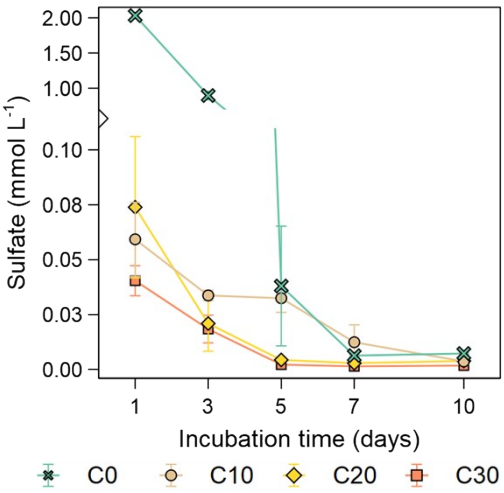

Figure S2: Time-resolved sulfate concentrations during the anoxic incubation period for all soils. Data points are average values and bars indicate standard deviation (n = 3).

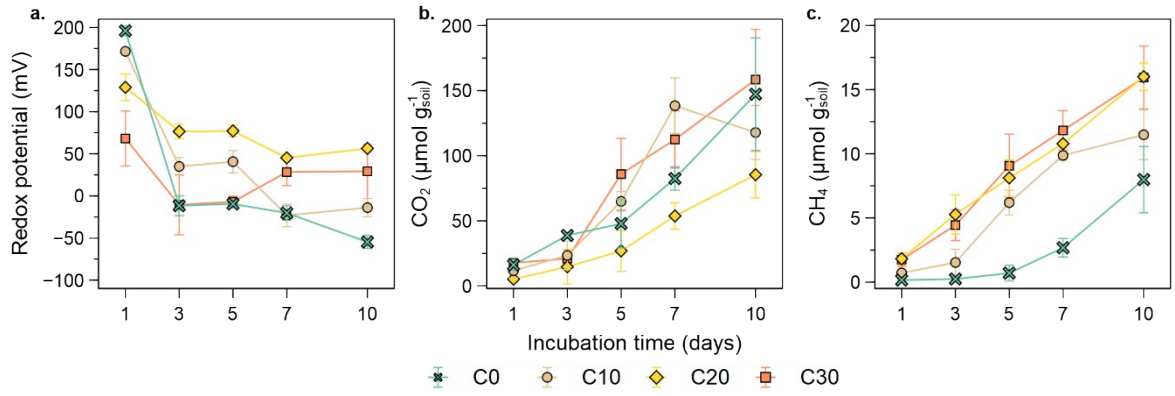

Figure S3: Temporal changes on redox potential (a), CO_2 production (b) and CH_4 production (c) for all redox cycled soils. Data points are average values and bars indicate standard deviation (n = 3).

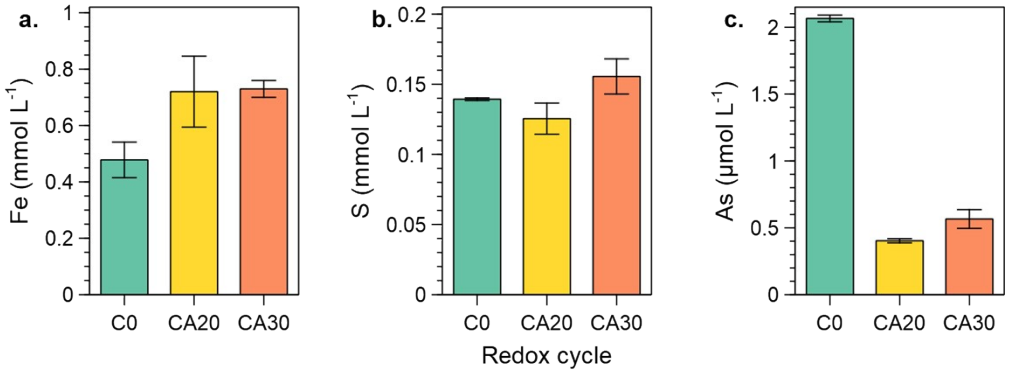

Figure S4: Comparison of aqueous phase Fe (a), S (b), and As (c) in C0 and constantly anoxic setups at day 10 of the anoxic cycle. Bar height is the average value, and bars indicate standard deviation (n = 3).

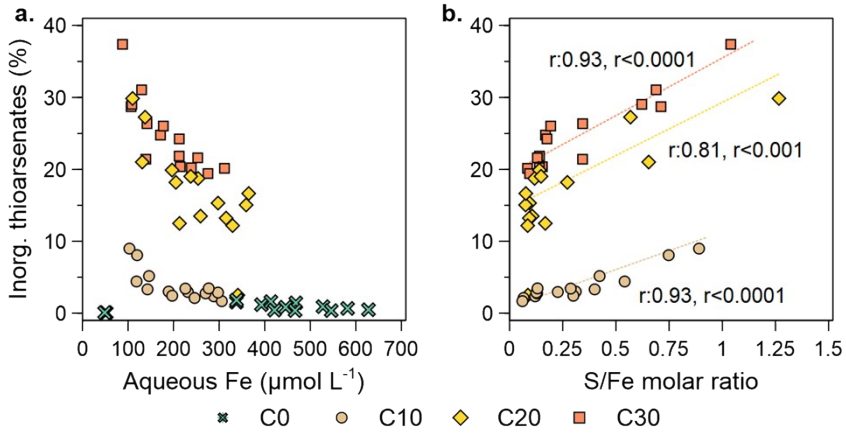

Figure S5: Influence of Fe depletion on thioarsenate formation in soils after repeated redox cycling (a) and effect of excess S over Fe on thioarsenate formation for each repleted soil (b).

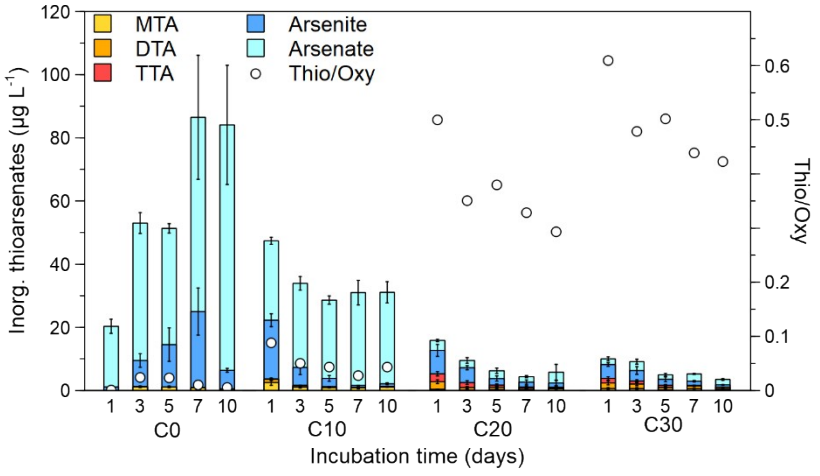

Figure S6: Temporal dynamics and contribution of all inorganic arsenic species to total As in the depleted soils.

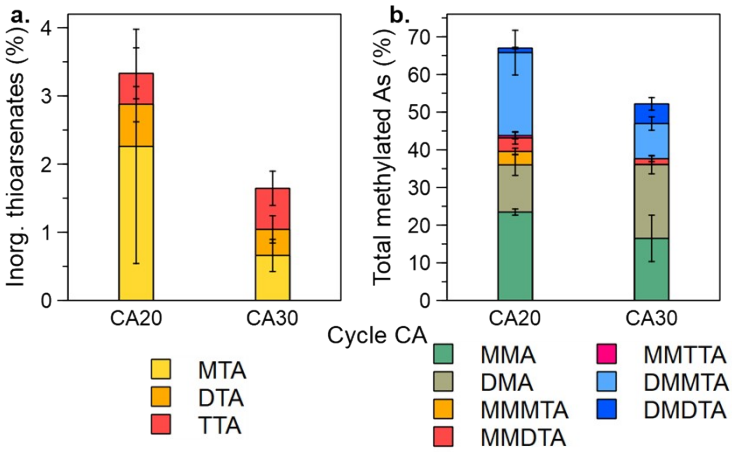

Figure S7: Inorganic thioarsenate and methylated As contribution to total As by anoxic incubation day 10 in CA setups.

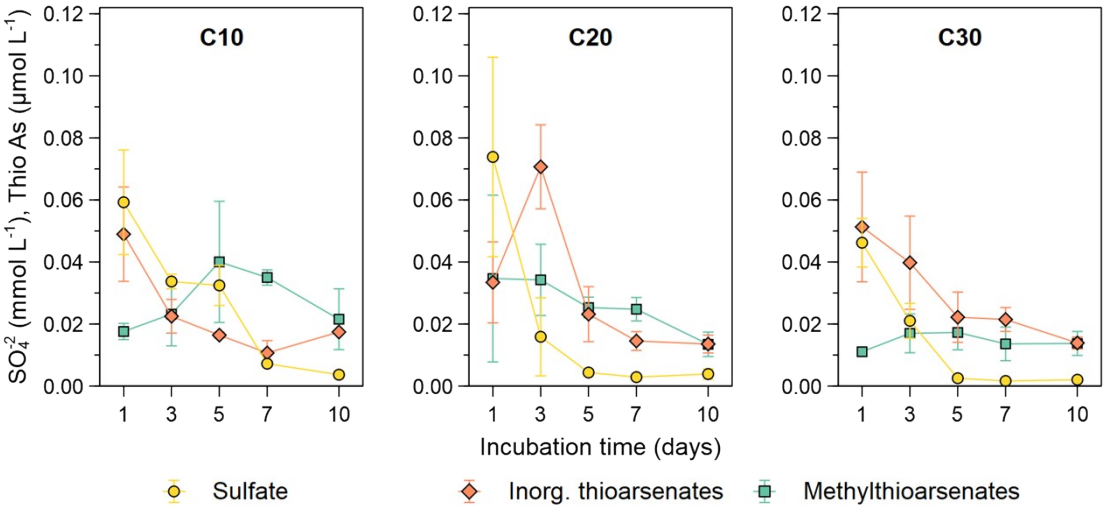

Figure S8: Temporal changes of inorganic and methylated thioarsenate concentrations in the soils after repeated redox cycling. Data points are average values and bars indicate standard deviation (n = 3).

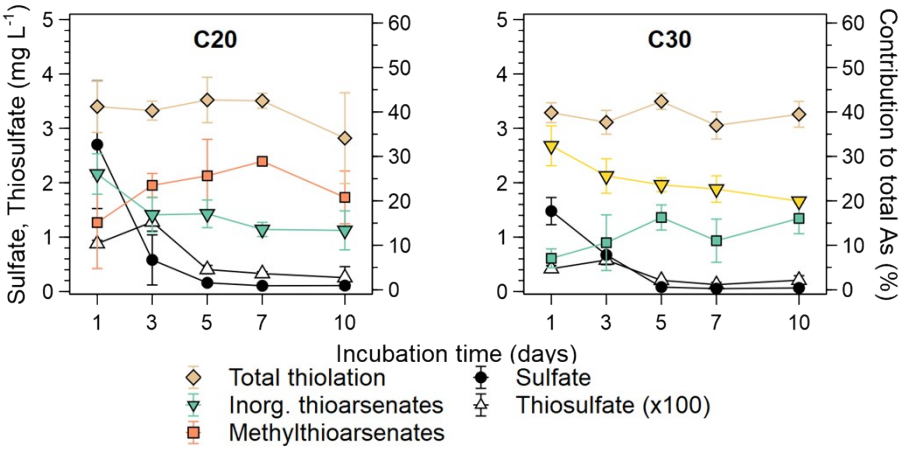

Figure S9: Temporal dynamics in the contribution of inorganic, methylated and total thiolated As species, and comparison with aqueous phase S species.Data points are average values and bars indicate standard deviation (n = 3).

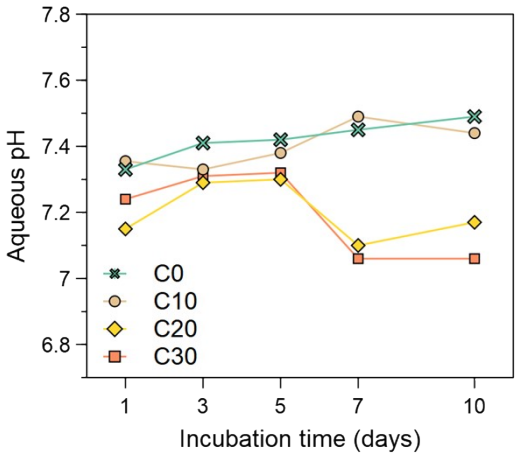

Figure S10: Temporal changes in aqueous phase pH with increasing redox cycling. Data points are average values and bars indicate standard deviation (n = 3).

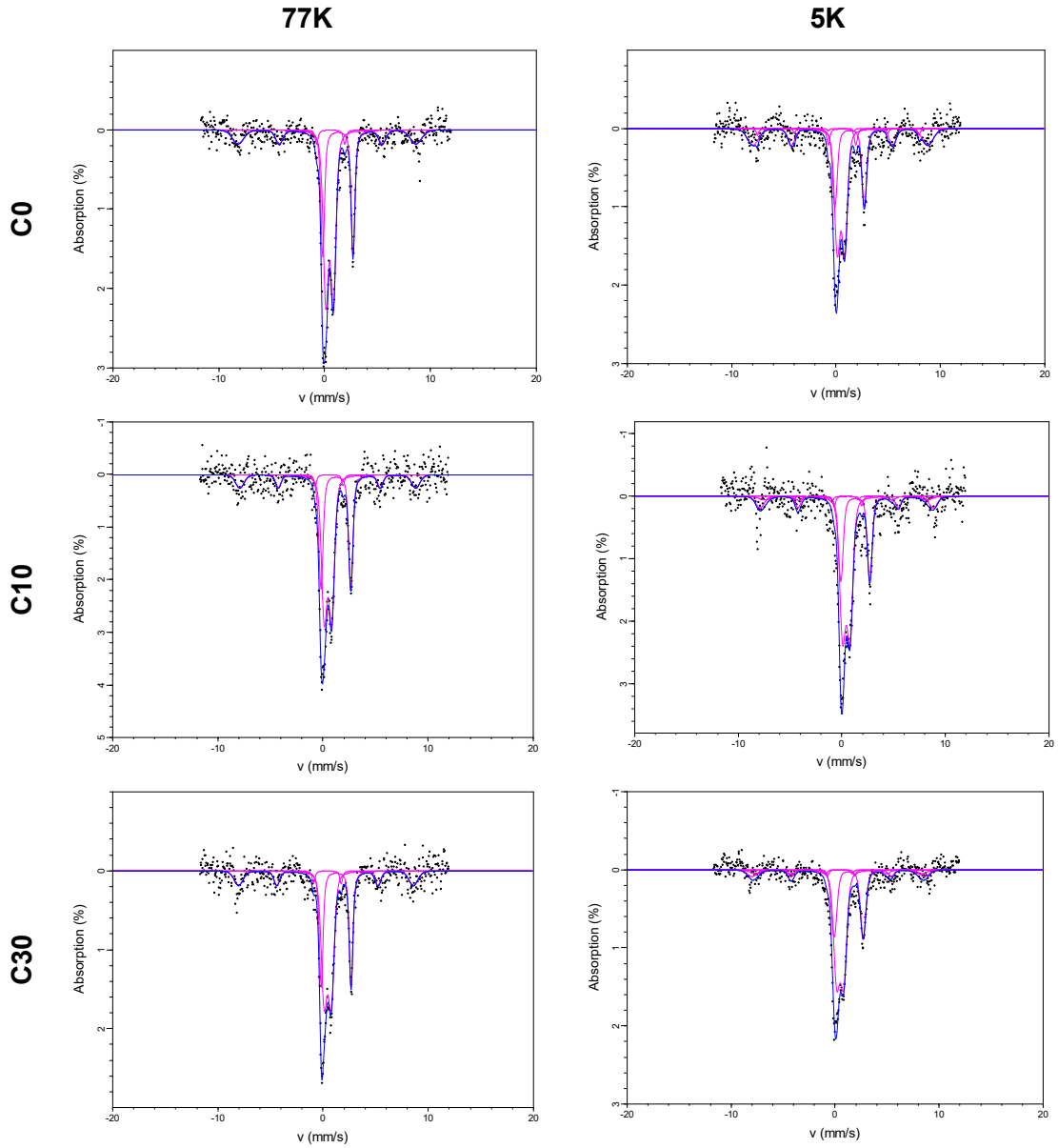

Figure S11: Mössbauer spectra and fitting of samples C0, C10, C30. Measurements taken at 77 and 5 K. Black dots show the original measurement. Blue and pink lines are the overall and individual fits, respectively.

Supplementary Discussion

Due to some uncertainties regarding the mineral phase of the Fe^{II} and the Fe^{III} (oxy)hydroxide, additional µXRD measurements were carried out (Figure S12). All samples were dominated by quartz. Therefore, some reflections were ambiguous. Other mineral phases found were wüstite ($Fe^{II}O$), siderite ($Fe^{II}CO_3$) and hematite ($Fe^{III}_2O_3$). Wüstite has a very similar pattern to periclase (MgO), so the main Fe^{II} phase was most likely siderite. The µXRD patterns did not show clear signs of clay minerals. However, the strong signal of quartz might have covered low abundant mineral phases.

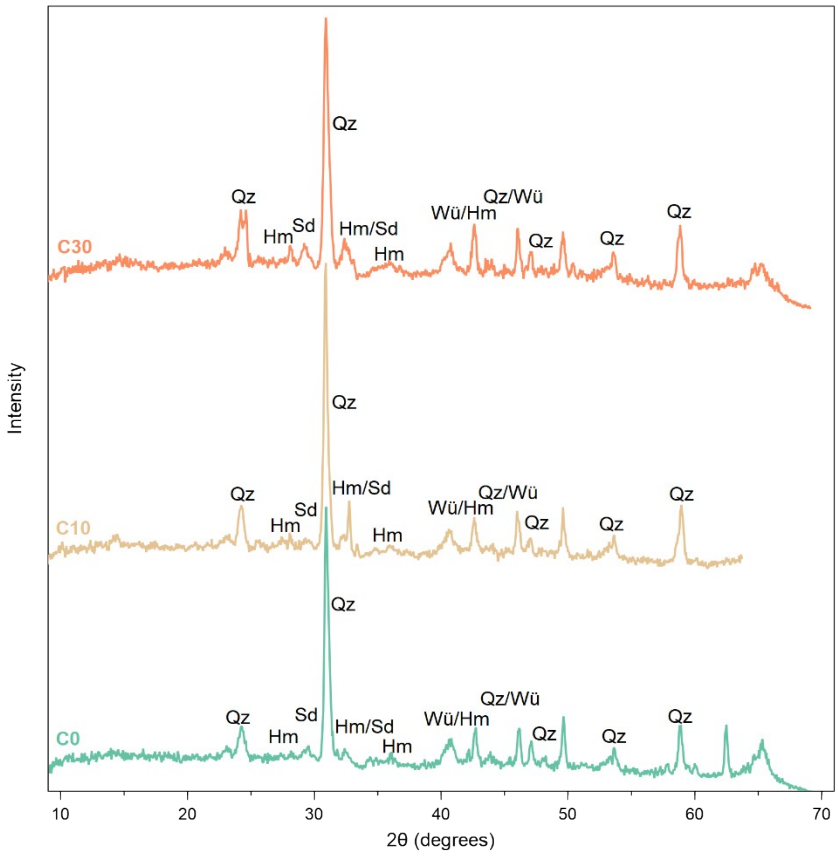

Figure S12: µXRD patterns of C0, C10, and C30 (from bottom to top). Quarz (Qz), Hematite (Hm), Siderite (Sd), Wüstite (Wü).

Supplementary References

1. Kölbl A, Schad P, Jahn R, Amelung W, Bannert A, Cao ZH, et al. Accelerated soil formation due to paddy management on marshlands (Zhejiang Province, China). Geoderma. 2014;228-229:67-89.
2. León Ninin JM, Muehe EM, Kölbl A, Higa Mori A, Nicol A, Gilfedder B, et al. Changes in arsenic mobility and speciation across a 2000-year-old paddy soil chronosequence. Science of The Total Environment. 2024;908:168351.